Journal of Applied Physics

Optically detected magnetic resonance of silicon vacancies in 4H-SiC at elevated temperatures toward magnetic sensing under harsh environments

Cite as: J. Appl. Phys. **133**, 154402 (2023); https://doi.org/10.1063/5.0139801
Submitted: 23 December 2022 • Accepted: 25 March 2023 • Published Online: 17 April 2023

Shu Motoki (元木 秀), **Shin-ichiro Sato** (佐藤 真一郎), **Seiichi Saiki** (佐伯 誠一), **et al.**

AIP Publishing

Journal of Applied Physics ARTICLE scitation.org/journal/jap

Optically detected magnetic resonance of silicon vacancies in 4H-SiC at elevated temperatures toward magnetic sensing under harsh environments

Cite as: J. Appl. Phys. **133**, 154402 (2023); doi: 10.1063/5.0139801
Submitted: 23 December 2022 · Accepted: 25 March 2023 ·
Published Online: 17 April 2023

View Online Export Citation CrossMark

Shu Motoki (元木 秀),[1,2,a)] Shin-ichiro Sato (佐藤 真一郎),[2] Seiichi Saiki (佐伯 誠一),[2] Yuta Masuyama (増山 雄太),[2] Yuichi Yamazaki (山崎 雄一),[2] Takeshi Ohshima (大島 武),[2] Koichi Murata (村田 晃一),[3] Hidekazu Tsuchida (土田 秀一),[3] and Yasuto Hijikata (土方 泰斗)[1]

AFFILIATIONS

[1]Graduate School of Science and Engineering, Saitama University, Saitama 338-8570, Japan
[2]National Institutes for Quantum Science and Technology, Takasaki, Gunma 370-1292, Japan
[3]Central Research Institute of Electric Power Industry, Yokosuka, Kanagawa 240-0196, Japan

[a)]**Author to whom correspondence should be addressed:** sato.shinichiro2@qst.go.jp

ABSTRACT

Negatively charged silicon vacancy (V_{Si}^-) defects in silicon carbide are expected to be used for magnetic sensors under harsh environments, such as space and underground due to their structural stability and potential for high-fidelity spin manipulation at high temperatures. To realize V_{Si}^- based magnetic sensors operating at high temperatures, the temperature dependence of optically detected magnetic resonance (ODMR) in the ground states of V_{Si}^- defects, which is the basic principle of magnetic sensing, should be systematically understood. In this work, we demonstrate the potential of V_{Si}^- magnetic sensors up to at least 591 K by showing the ODMR spectra with different temperatures. Furthermore, the resonance frequency of the ground level was independent of temperature, indicating the potential for calibration-free magnetic sensors in temperature-varying environments. We also characterize the concentration of V_{Si}^- defects formed by electron irradiation and clarify the relationship of magnetic sensing sensitivity to V_{Si}^- concentration and find that the sensing sensitivity increases linearly with V_{Si}^- concentration up to at least $6.0 \times 10^{16}\,\mathrm{cm}^{-3}$. The magnetic sensitivity at a temperature above 549 K was reduced by half as compared to that at 300 K. The results pave the way for the use of a highly sensitive V_{Si}^--based magnetic sensor under harsh environments.

I. INTRODUCTION

Optically active spin defects in silicon carbide (SiC) have attracted attention as "quantum sensors" that can detect magnetic fields and temperatures with a wide-dynamic range, high resolution, and high sensitivity. A single-negatively charged silicon vacancy (V_{Si}^-) is a promising spin defect in SiC for quantum sensors and, consequently, magnetic sensing using V_{Si}^- has been extensively studied.[1–3] Compared to the nitrogen-vacancy (NV) center in diamond, which is the best-known quantum sensor,[4–8] V_{Si}^- emits luminescence at near-infrared (NIR) wavelengths (800–1100 nm),[3,9] which reduces scattering losses at interfaces and signal attenuation in optical fibers. The half-integer spin $S = 3/2$ in V_{Si}^- (Refs. 1, 10, and 11) is controllable and optically detectable on a single spin level at room temperature with a long spin coherence time.[12] The principle of magnetic sensing with V_{Si}^- is usually based on optically detected magnetic resonance (ODMR), where magnetic fields are detected by analyzing the change in the emission intensity from optically excited defects. The resonance frequencies of the ground states between $m_s = \pm 1/2$ and $m_s = \pm 3/2$ in V_{Si}^- vary with the magnetic field due to the Zeeman effect, resulting in highly sensitive atomic-scale magnetic sensing.

Unlike NV centers in diamond, SiC quantum sensors can be realized at a reasonable cost because large-diameter (200 nm) and high-quality (electronic grade, i.e., high purity and low defect density) SiC wafers are commercially available.[13–16] In addition, integration of V_{Si}^- quantum sensors with photonic devices and SiC CMOS integrated circuits can be expected by utilizing mature nanofabrication and device technologies. Recently, it has been demonstrated that the photon collection efficiency of photon emission from single V_{Si}^- centers in 4H-SiC was improved by incorporating them into the scalable array of nanopillars,[17] and the Purcell enhancement of a single V_{Si}^- center was achieved by coupling it to a nano-beam photonic crystal cavity.[18] On the other hand, electron spin states of V_{Si}^- on 4H-SiC metal–oxide–semiconductor field effect transistors (MOSFETs) have been detected at room temperature using electrically detected magnetic resonance (EDMR),[19] and all-electric magnetic sensors based on deep-level defects in 4H-SiC pn-junction devices have been proposed.[20] We have demonstrated the successful introduction of electrically controllable V_{Si}^- into SiC pn-diodes without significant performance degradation,[21] and its temperature change during diode operation has been detected by V_{Si}^- quantum sensors.[22] These results are an important step toward the practical implementation of V_{Si}^- quantum sensor devices, suggesting that further research will accelerate the realization of industrial applications.

We also strongly anticipate that V_{Si}^- in 4H-SiC can be used for magnetic sensors operating in harsh environments, such as space and underground due to its structural stability at high temperatures.[3,23–25] Magnetic sensors mounted in satellites are subjected to thermal cycling (e.g., −120 to +150 °C) as well as strong radiation, which prevents long-term stable operation.[26] In addition, tolerance to high temperatures above 450 °C is necessary for the exploration of the interior planets, such as Venus and Mercury.[27] Therefore, the development of robust sensors that are not by temperature is essential for future space applications. V_{Si}^- in 4H-SiC is a strong candidate for robust magnetic sensors that allow temperature-insensitive, long-term, and high-temperature operation without any measurement calibration, although the magnetic sensing using V_{Si}^- at high temperatures and the temperature dependence of magnetic sensitivity have been little been discussed.

High-energy electron irradiation is commonly used to create V_{Si}^- defects in SiC.[1,12] V_{Si}^- defects increase and its magnetic sensitivity improves with increasing electron fluence, although unwanted paramagnetic defects that induce decoherence of V_{Si}^- also increase. There is still a lack of information on the relationship between V_{Si}^- concentrations and the ODMR properties in SiC irradiated with a wide range of electron fluence. The method of V_{Si}^- formation to maximize the sensing performance has not been well studied.

In this work, we experimentally demonstrate that V_{Si}^- magnetic sensors can be operated at least up to 591 K by showing the ODMR spectra at different temperatures and different V_{Si}^- concentrations. We clarify that the resonance frequency of zero-field splitting in the ground state of V_{Si}^- is unchanged by this temperature, although the ODMR contrast decreases with increasing temperature. We also evaluate the magnetic sensitivity as a function of temperature and clarify that the magnetic sensitivity can maintain considerable sensitivity even at temperatures above 549 K as compared to that at 300 K. Furthermore, we investigate the relationship between V_{Si}^- concentration and magnetic sensitivity over a wide range.

II. EXPERIMENTAL

High purity semi-insulating (HPSI) 4H-SiC substrates and n-type 4H-SiC epi-layers were irradiated with 2 MeV electrons at ambient temperature to create V_{Si}^- defects uniformly over the substrate surface. Epitaxial growth was conducted with a vertical hot-wall CVD reactor using commercial 4° off 4H-SiC (0001) Si-face substrates.[28] An H_2-HCl-SiH_4-C_3H_8 gas system was employed, and an N_2 gas was used for N doping. The samples were mounted on a water-cooled copper (Cu) plate and covered with an 11 μm-thick aluminum (Al) foil during irradiation. Fluences ranging from 1.2×10^{15} to 1.3×10^{19} cm^{-2} were chosen to study the irradiation fluence dependence. After irradiation, some of the samples were thermally annealed at 600 °C for 30 min in a vacuum to confirm the high-temperature stability of V_{Si}^- defects. The sample information is summarized in Table I.

Electron spin resonance (ESR) measurement at room temperature without light illumination was performed with an X-band ESR spectrometer (JES-X330, JEOL Ltd.) to investigate the V_{Si}^- concentration formed by electron irradiation. To quantify the number of spins, the doubly integrated intensity of a differential ESR spectrum was compared with that of a deliberately quantified standard of copper sulfate pentahydrate ($CuSO_4 \cdot 5H_2O$). The V_{Si}^- defect concentration was derived from the sample weight and the number of spins.

In addition to the ESR measurement, deep-level transient spectroscopy (DLTS) analyses were performed to determine the concentration of the V_{Si} defects (S_1 centers), employing Ni metal pads of 1 mm diameter as Schottky contacts and an Al thin film as a backside Ohmic contact. For the measurement, the rate window of 41 or 410 ms and the pulse width of 50 ms were applied. The applied voltage was −10 V.

The photoluminescence (PL) and ODMR properties of V_{Si}^- were characterized using a home-built confocal fluorescence microscope (CFM) equipped with a temperature variable stage (80–600 K), the signal generator [Agilent, E4428C (250 kHz–3.0 GHz)], and the amplifier [Mini-Circuits, LZY-22+ (100 kHz–200 MHz)]. A schematic diagram of the experimental setup for PL and ODMR measurements is shown in Fig. 1. A 785 nm CW-laser,

TABLE I. Sample information.

Sample	Doping conc. (cm^{-3})	2 MeV-e fluence (cm^{-2})	Postanneal	Characterization
HPSI 4H-SiC	NA	1.2×10^{15}–1.3×10^{19}	NA	ESR, PL, TRPL, ODMR
HPSI 4H-SiC	NA	5.8×10^{17}–3.4×10^{18}	600 °C, 30 min	ESR, PL,ODMR
n-type 4H-SiC	2×10^{17}	1.2×10^{16}–1.2×10^{17}	600 °C, 30 min	DLTS

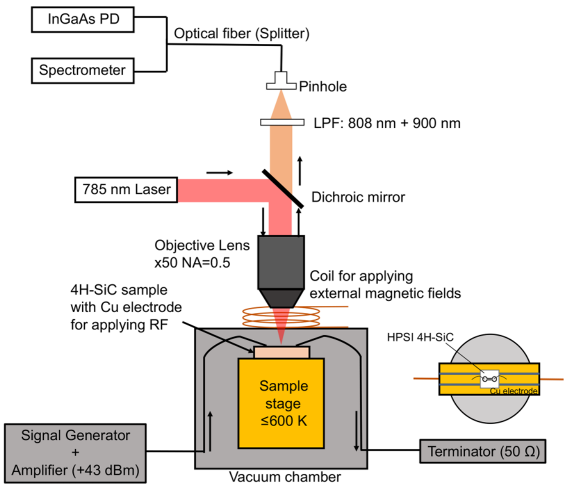

FIG. 1. A schematic of the experimental setup for PL and ODMR. A top view of the sample stage is also shown on the right.

which is close to the optimal excitation wavelength,[29] was used with an objective lens (×50, NA = 0.5) for optical excitation. The laser power was 45 mW, and the spot diameter was estimated to be 1.9 μm. The emitted photons from V_{Si}^- were collected by an InGaAs photodiode or an imaging spectrometer through an optical fiber after removing other photons with long-pass filters at 808 and 900 nm. For the ODMR measurement, a 40 μm wide Cu electrode was deposited on the sample surface by a sputtering method to apply a radio-wave frequency (RF). The RF signals in the circuits were checked with a spectrum analyzer prior to the ODMR measurements. A μ-metal plate is placed on the sample stage to minimize the effect of magnetic noise generated by a heater installed in the stage. For repeatability, the measurement location was fixed to 20 μm laterally from the electrode edge and 20 μm deep from the surface (see the supplementary material for details).

To analyze the temperature dependence of the fluorescence lifetime of V_{Si}^- defects, time-resolved photoluminescence (TRPL) was measured using time-correlated single-photon counting (TCSPC).[29] In this experiment, a 700 nm pulsed laser was used for optical excitation, and PL decay was detected by a Si single-photon avalanche photodiode through an 808 nm long-pass filter.

III. RESULTS AND DISCUSSIONS

A. Concentration of V_{Si}^-(k) defects formed by electron irradiation

We first analyzed the MW power dependence of the ESR integrated intensity for accurate characterization of T_{V2a} center (V_{Si} defect) concentration, and the MW power of 0.4 μW was used for all the samples (see the supplementary material for details). Figure 2 shows the ESR spectrum of electron-irradiated SiC at the fluence of 5.0×10^{18} cm^{-2}. Note that the V_{Si}^- in 4H-SiC has two different sites (k- and h-site), which show different ESR spectra in Fig. 2(a). The ESR spectra for T_{V1a} and T_{V2a} centers have been identified as V_{Si}^- at the h-site [V_{Si}^-(h)] and V_{Si}^- at the k-site [V_{Si}^-(k)], respectively.[30,31] V_{Si}^- defects (S = 3/2) show three equivalent peaks due to the allowed transition between four spin energy states ($m_S = +3/2, \ +1/2, \ -1/2, \ -3/2$). Each peak shows small splits due to the hyperfine structure of ^{29}Si. The ESR spectra of V_{Si}^- in Fig. 2(a) can basically be explained as the superposition of V_{Si}^-(h) and V_{Si}^-(k) with different splitting widths. Since the resonances at the ground level of V_{Si}^-(k) are used for magnetic sensing, we focused only on the concentration of V_{Si}^-(k).[2,32] To quantify V_{Si}^-(k) defects, we extracted the left peak of the ESR spectrum of T_{V2a} shown in Fig. 2(b) and calculated the number of spins of V_{Si}^-(k) as three times the number of spins of the left peak.

The V_{Si}^-(k) concentration as a function of irradiation fluence from 1.1×10^{17} to 1.3×10^{19} cm^{-2} is shown in Fig. 3(a). The V_{Si}^-(k) concentration increased linearly with increasing irradiation fluence with a slope of 1.01 ± 0.11 and no saturation behavior appeared up to 1.3×10^{19} cm^{-2}, indicating that higher V_{Si}^-(k) concentration is achievable by further electron irradiation. It should be noted that the total concentration of V_{Si}^- defects [sum of V_{Si}^-(k) and V_{Si}^-(h)] is expected to be doubled because their concentrations are assumed to be comparable. Below 1.1×10^{17} cm^{-2} of irradiation

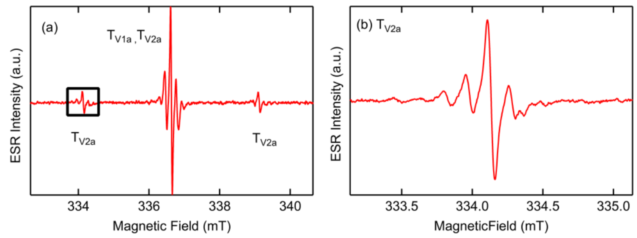

FIG. 2. (a) Typical ESR spectrum of V_{Si}^- in 4H-SiC for B || c at room temperature [electron fluence: 5.0×10^{18} cm^{-2}, microwave power: 0.4 μW, modulation field: 0.05 mT, and modulation frequency: 100 kHz]. (b) Magnified ESR spectrum of the left peak of the T_{V2a} center.

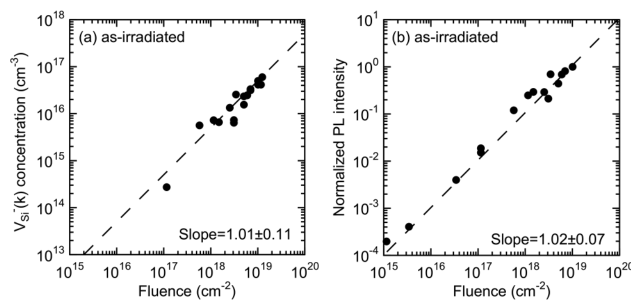

FIG. 3. (a) V_{Si}^-(k) concentration as a function of irradiation fluence from 1.1×10^{17} to 1.3×10^{19} cm^{-2}. Closed symbols are experimental data for as-irradiated samples. The dashed line is the least-squares fit to $[V_{Si}^-(k)] = C e^{\alpha}$ with $\alpha = 1.01 \pm 0.11$. (b) Normalized PL intensity as a function of irradiation fluence at room temperature from 1.1×10^{15} to 1.3×10^{19} cm^{-2}. The PL intensity is normalized by the value at 1.3×10^{19} cm^{-2}. The least-squares fit to the experimental data is shown as a dashed line with a slope of 1.02 ± 0.07.

fluence, the $V_{Si}^-(k)$ concentration could not be calculated accurately because the signal-to-noise (S/N) ratio was too low. However, it is possible to estimate the $V_{Si}^-(k)$ concentration at the low irradiation fluence by the PL intensity. Figure 3(b) shows the normalized integrated PL intensity (integral range: 800–1100 nm) at room temperature as a function of irradiation fluence from 1.1×10^{15} to 1.3×10^{19} cm^{-2}. We assume that the PL intensity ratio of $V_{Si}^-(k)$ to $V_{Si}^-(h)$ defects was constant with the electron irradiation. Similar to the quantification of $V_{Si}^-(k)$ concentration by ESR spectra, the PL intensity increased linearly with increasing irradiation fluence with a slope of 1.02 ± 0.07. This indicates that the $V_{Si}^-(k)$ concentrations below the irradiation fluence of 1.1×10^{17} cm^{-2} can be estimated by the relative change of the PL intensity. Some data fluctuations in the PL intensities can be seen in Fig. 3, and we estimate that this is due mainly to the error of the electron irradiation fluence (roughly 10%).

In addition to ESR and PL measurements, DLTS measurements were employed to further analyze the concentration of created V_{Si} defects and their dominant charge states (see the supplementary material for the detail of the DLTS measurements). Figure 4 shows a comparison of the V_{Si} concentrations determined by DLTS and ESR for the samples annealed at 600 °C. In DLTS measurements, all V_{Si} defects are detected as the S_1 center regardless of their dominant charge state in equilibrium.[33,34] Since the signal from the S_1 center (V_{Si} defects) overlaps with that from other centers, such as $EH_1(E_1)$ centers and M centers [originating from inter-lattice carbon defects (C_i)], which disappear or change to other defects upon low-temperature annealing (200–400 °C),[35–40] we performed 600 °C annealing before the DLTS measurements to properly characterize the S_1 centers. The results showed that the S1 concentration increased linearly with increasing electron fluence, as shown by the blue symbols in Fig. 4. Then, four of the electron-irradiated HPSI 4H-SiC samples were annealed at 600 °C, and their V_{Si}^- concentrations (i.e., twice the concentration of T_{V2a} centers) were identified by the ESR measurement. After annealing at 600 °C for 30 min, the V_{Si}^- defects were reduced to about 70% of the non-annealed samples. The obtained values (twice the concentration of T_{V2a} centers) are plotted as closed red symbols in Fig. 4, being on the straight line extrapolated from the DLTS data. The least-squares fit to the experimental data are drawn as a dashed line with a slope of 1.01 ± 0.12. This fit line is 1.4 (=2 × 0.7) times higher than the fit line shown in Fig. 3(a), which is consistent with the results from unannealed samples. This fact indicates that most of the V_{Si} defects formed in electron-irradiated HPSI 4H-SiCs are single negatively charged.[41] The results also indicate that the initial impurity doping did not affect the number of V_{Si} defects formed by electron irradiation and that the same amounts of $V_{Si}(k)$ and $V_{Si}(h)$ were formed.

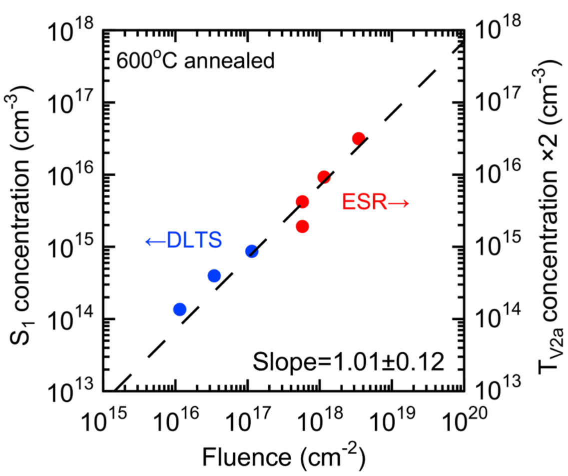

FIG. 4. Comparison of the V_{Si} concentrations (600 °C annealed samples) derived from DLTS and ESR measurements. Closed blue symbols denote the results obtained by DLTS signals (S_1 centers). The doping concentrations are 2×10^{17} cm^{-3}. Closed red symbols are the results obtained by ESR signals (T_{V2a} centers). Note that the right ordinate is twice the value of the T_{V2a} [$V_{Si}^-(k)$] concentration. The least-squares fit to the experimental data is shown as a dashed line with a slope of 1.01 ± 0.12.

B. Optical properties and spin manipulations

The photoluminescence properties of V_{Si}^- defects were investigated at elevated temperatures. Figure 5 shows the PL spectra measured at temperatures ranging from 300 to 591 K. The electron irradiation fluence was 7.0×10^{18} cm^{-2} ($[V_{Si}^-(k)] = 3.3 \times 10^{16}$ cm^{-3}), and no annealing was performed after irradiation. Broad emission centered at around 900 nm appeared at temperatures above 300 K. This is attributed to the phonon sidebands (PSBs), and zero phonon lines (ZPLs) were not observable at these temperatures.[3,9] The ZPLs originating from $V_{Si}^-(h)$ and $V_{Si}^-(k)$ defects (V1 and V2 peaks, respectively) were found at 80 K (see the supplementary material). The PL intensity around 820–870 nm increased with increasing temperature due to the broadening of the PSBs. Interestingly, the integrated PL intensity slightly increased by a factor of 1.05 ± 0.01 at 591 K compared to the intensity at 300 K. A similar trend was

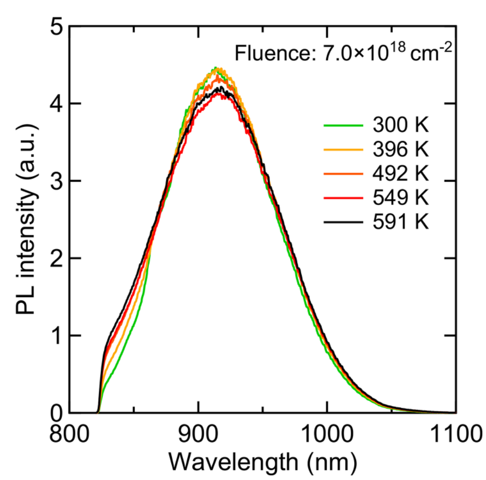

FIG. 5. PL spectra at different temperatures from 300 to 591 K.

found in the other samples with different V_{Si}^-(k) concentrations (see the supplementary material for details).

A representative PL decay curve for V_{Si}^- with the concentration of $1.7 \times 10^{16}\,cm^{-3}$ after pulsed excitation at 300 K is shown in Fig. 6(a). Note that the photon emission decay for both V_{Si}^-(h) and V_{Si}^-(k) defects was characterized in this measurement since the wavelength above 808 nm was collected. The experimental data are fitted with a mono-exponential decay function in the form of $a + b \times \exp(-t/\tau)$. The PL lifetime, τ, was determined from the fit to be 6.3 ns, which agrees well with the previous report (6.1 ns).[29] Figure 6(b) shows the PL lifetime V_{Si}^- as a function of temperature. The PL lifetime slightly increased with increasing temperature up to 400 K and slightly decreased above it. A similar trend was found in the other samples with different V_{Si}^- concentrations.

The Mott–Seitz model can explain the temperature dependence of the lifetime of color centers, including V_{Si}^-.[8,42] In this model, the nonradiative transition rate (k_{NR}) increases with increasing temperature, and the measured lifetime (τ_M) is shortened; $1/\tau_M = 1/\tau_{Rad} + k_{NR}$, where τ_{Rad} is the radiative transition lifetime. However, the Mott–Seitz model cannot explain the measured lifetimes below 300 K, which decrease with decreasing temperature, as shown in Fig. 6(b). $Z_{1/2}$ centers (carbon vacancies, V_C[43]) are known to be the dominant limiting factor for carrier recombination lifetimes in electron-irradiated SiC, and thus, the lifetime of V_{Si}^- centers could also be affected by the surrounding $Z_{1/2}$ centers. Charge transfer between V_{Si}^- and V_C^+ (i.e., $V_{Si}^- + V_C^+ \rightleftarrows V_{Si}^0 + V_C^0$), resulting in the change in a lifetime, may be possible since the dominant charge state of V_C in HPSI 4H-SiC is +1.[41] Another possibility is that the lifetime of V_{Si}^- centers can be affected by an interaction with free carriers (electrons in the conduction band and holes in the valence band) in the SiC host. It has been reported that the recombination lifetime of free carriers in SiC increases with increasing temperature up to 300–400 K and then decreases at higher temperatures.[44,45] This trend is opposite to the measured lifetime of V_{Si}^- centers and may be related to the interaction between V_{Si}^- centers and free carriers. Assuming the existence of carrier transfer from an SiC host to V_{Si}^- centers and of the photo-excited carriers generated via defect levels (e.g., V_C centers) during 700 nm laser irradiation,[46] the lifetime of V_{Si}^- centers could be short due to the carrier transfer to an SiC host when the recombination lifetime of free carriers is long. Further investigation is needed to clarify the origin of the lifetime variation with temperature.

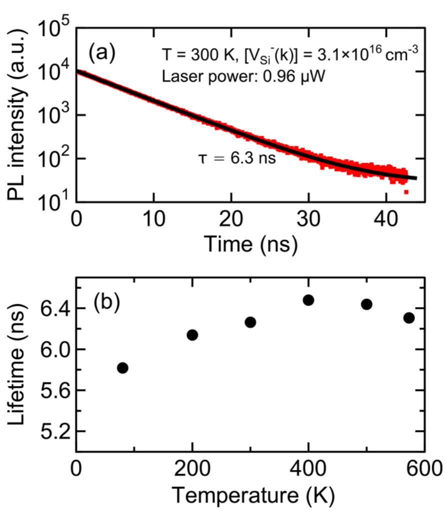

FIG. 6. (a) A representative PL decay curve of V_{Si}^- defects. The mono-exponential decay fit with a characteristic lifetime τ = 6.3 ns is shown as the solid line. (b) The PL lifetime as a function of temperature.

Figure 7(a) shows the ODMR spectra of V_{Si}^-(k) defects measured at different temperatures (from 80 K to 591 K) under a zero magnetic field. Since only the spin state of the V2 center [V_{Si}^-(k) defects], whose ZPL is 916 nm, can be manipulated by applying RF,[32] ODMR measurements were performed through a 900 nm LPF. The electronic ground state of the V_{Si}^- defects is a quartet manifold, S = 3/2, and the Hamiltonian is

$$H = D\left[S_Z^2 - S(S+1)/3\right] + g\mu_B B S_Z, \tag{1}$$

where $2D = 70$ MHz is the zero-field splitting (ZFS) parameter between $m_S = \pm 3/2$ and $m_S = \pm 1/2$, $g = 2.0032$ is the electron g-factor,[47] μ_B is the Bohr magnetron, and B is the applied axial static magnetic field. The spin states degenerate under zero magnetic field. A resonance peak due to ZFS (=2D) of the ground level was seen at around 70 MHz at room temperature (300 K), which was in good agreement with the previous works.[1–3,32,48] Resonance peaks were clearly observed even up to at least 591 K, indicating that V_{Si}^-(k) spins can be manipulated even at high temperatures. The resonance frequency was unchanged by temperature, with an average resonance frequency of 69.5 ± 0.2 MHz. The ODMR contrast, which is calculated as the RF-induced PL change (ΔPL) divided by the PL intensity, i.e., ΔPL/PL, decreased with increasing temperature as shown in Fig. 7(b). The decrease in the ODMR contrast is presumably due to the decrease in the spin polarization rate with increasing temperature as well as the thermally activated non-radiative processes, which would diminish the fluorescence-based spin readout.[8,49] Figure 7(c) shows the full width at half maximum (FWHM) of the ODMR spectra as a function of temperature.

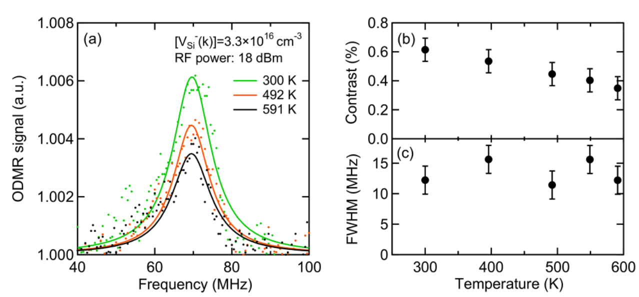

FIG. 7. Temperature dependence of the ODMR spectra. (a) ODMR spectra of V_{Si}^- at different temperatures (from 300 to 591 K) under zero magnetic field. Solid curves represent fits with the Lorentzian function. (b) Contrast (%) and (c) FWHM (MHz) extracted from the ODMR spectra, respectively. The uncertainties of the ODMR contrast (±0.08) and FWHM (±2.3 MHz) are shown as error bars.

The FWHM is independent of temperature, suggesting that the coherent properties of V_{Si}^{-}(k) defects are maintained at high temperatures.

According to Eq. (1), when an external magnetic field is applied for B||c, the spin sublevels split due to the Zeeman splitting. Two resonance transitions, $m_S = -1/2 \Leftrightarrow m_S = -3/2$ and $m_S = +1/2 \Leftrightarrow m_S = +3/2$ whose corresponding resonance frequencies are $\upsilon 1 = |2D - g\mu_B B|$ and $\upsilon 2 = 2D + g\mu_B B$, mainly appear.[2] Figures 8(a) and 8(b) show the ODMR spectra of V_{Si}^{-}(k) defects measured without and with external magnetic fields (B = 0 and 1 mT) for B||c at 300 and 591 K. The resonance frequencies of the ODMR signal as a function of the magnetic field for B||c from 0 to 5 mT are shown in Fig. 8(c). The experimental results are in good agreement with the theoretical calculation values at both temperatures.[2,30,48] This fact indicates that V_{Si}^{-}-based quantum sensors are capable of magnetic sensing over a wide temperature range without temperature calibration. Unlike the other promising candidates for quantum sensors, such as NV centers in diamond,[5,6,8] divacancy ($V_{Si}V_C^{0}$) defects in SiC,[50] and a negatively charged boron vacancy (V_B^{-}) in hexagonal boron nitride (h-BN),[51] no frequency adjustment for measurement calibration is required for V_{Si}^{-}(k) magnetic sensors when operated under temperature variable conditions.

We also investigated the effects of γ-ray irradiation on the PL and ODMR properties to demonstrate the radiation resistance of V_{Si}^{-}(k) magnetic sensors (see the supplementary material for details). As a result, no significant change was found in the PL and ODMR properties of V_{Si}^{-}(k) defects at least up to 119 kGy (H_2O), and this fact strongly indicates that V_{Si}^{-}(k) magnetic sensors can be used in a radiation environment without any deterioration.

C. Magnetic sensitivity

The magnetic sensitivity of the ODMR magnetometer is typically limited by the shot-noise sensitivity that is related to the minimum detectable magnetic field.[7] The shot-noise-limited DC magnetic field sensitivity, η, is represented by

$$\eta = \frac{4\hbar}{3\sqrt{3}g_e\mu_B} \times \frac{\Delta\upsilon}{C\sqrt{R}} \left(T/\sqrt{Hz}\right), \tag{2}$$

where $\hbar$ is Planck's constant, g_e is Landé's g-factor, μ_B is Bohr's magnetron, R is the photon-detection rate, $\Delta\upsilon$ is the FWHM of the ODMR signal, and C is the contrast of the ODMR signal. The FWHM is inversely proportional to the spin dephasing time of the defect, T_2*. C and R depend on many terms, such as the Rabi frequency (RF power), the transition rate, defect brightness, and optical collection efficiency. R was calculated from the intensity of the detector (InGaAs PD) and its spectral response. Figure 9(a) shows the normalized shot-noise-limited sensitivity as a function of V_{Si}^{-}(k) concentration at room temperature. The shot-noise-limited sensitivity was normalized to the value of V_{Si}^{-}(k) concentration of 2.3×10^{16} cm^{-3}. The magnetic sensitivity was linearly reduced with the increase in V_{Si}^{-}(k) concentration with a slope of -0.50 ± 0.11. The maximum shot-noise-limited sensitivity obtained in our study was estimated to be 125 nT/$\sqrt{\text{Hz}}$ at the V_{Si}^{-}(k) concentration of 6.0×10^{16} cm^{-3} (electron irradiation fluence of 1.3×10^{19} cm^{-2}). The number of measured V_{Si}^{-}(k) defects was roughly estimated to be 4.3×10^{5} from the net laser spot size and the concentration. In addition, no significant change was found in the magnetic sensitivity after thermal annealing at 600 °C for 30 min in a vacuum, indicating the high-temperature stability of V_{Si}^{-} magnetic sensors. After thermal annealing at 600 °C for 30 min in a vacuum, the V_{Si}^{-}(k) concentration decreased by 70% (Fig. 4) and the photon-detection rate decreased accordingly, resulting in the sensitivity degradation. The data for annealed samples, shown as red closed triangles in Fig. 9(a), also follow the linear fit. However, a significant decrease in the PL intensity at temperatures above 700 °C has been reported in previous reports.[3,23,25] The V_{Si} defects are annihilated or transformed into complex defects at temperatures above 700 °C, although a part of them is retained. Figure 9(b) shows the change in shot-noise-limited sensitivity as a function of temperature (300–591 K) at the V_{Si}^{-}(k) concentration of 3.3×10^{16} cm^{-3}. The shot-noise-limited sensitivity was normalized to the value of 300 K. The magnetic sensitivity deteriorated by a factor of 2 at temperatures above 549 K. The relative sensitivity change with temperature can be compared to other spin defects, such as NV centers in diamond, although the magnetic sensitivity at high temperature has not been reported. According to Ref. 8, the ODMR contrast and the PL intensity of NV centers decrease with increasing temperature, and the decrease ratio of 550 to 300 K is 50% and 30%, respectively. On the other hand, the spin coherence time (T_2*) is not affected by temperature, indicating that the FWHM of the ODMR signal is constant. From these data, the shot-noise-limited magnetic sensitivity is estimated to be reduced by about 30% at 550 K as compared to that at 300 K, which is lower than that of V_{Si}^{-}(k) defects (about half). Considering this fact and the temperature independent resonance frequency, the magnetic sensing of V_{Si}^{-} defects may be more advantageous than NV centers in high temperature and thermal cycling conditions, such as space environments.

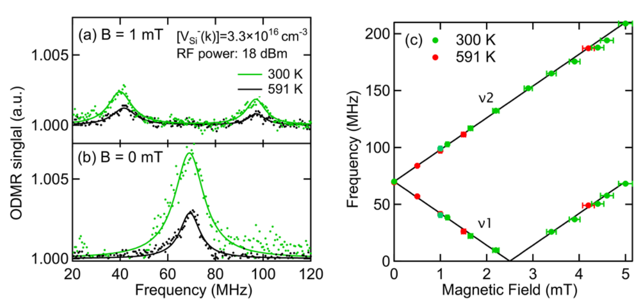

FIG. 8. ODMR spectra at 300 and 591 K for (a) B = 0 mT and (b) B = 1 mT (B|| c). (c) The resonance frequency of the V_{Si}^{-} ground states as a function of magnetic field for B || c. Green and red symbols are the experimental data at 300 and 591 K, respectively. The theoretical values, whose slopes are 28 MHz/mT, are represented by solid lines. The uncertainties of the resonance frequency (±0.6 MHz) and the magnetic fields (±3%) are shown as error bars.

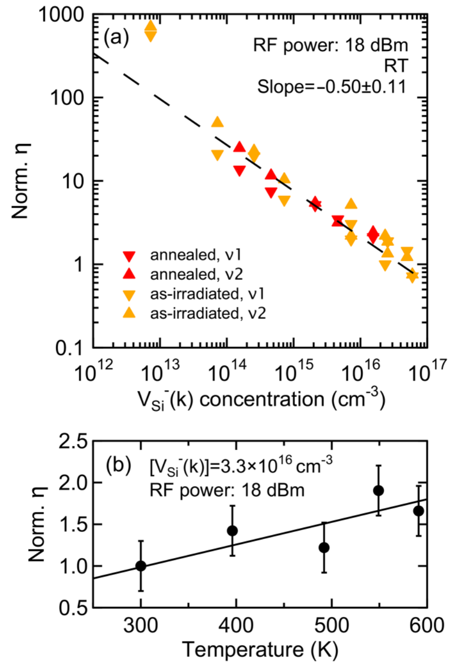

FIG. 9. V_{Si}^-(k) concentration and temperature dependence of the shot-noise-limited sensitivity (η). (a) Normalized η as a function of V_{Si}^-(k) concentration at room temperature. Red and yellow triangles are the results for 600 °C annealed and as-irradiated samples, respectively. The least-squares fit to the experimental data (except for the data at 7.3×10^{12} cm^{-3}) is shown as a dashed line with a slope of -0.50 ± 0.11. (b) Normalized η as a function of temperature. The solid line is drawn to guide the eye.

Although the best sensitivity obtained in this study was 125 nT/$\sqrt{\text{Hz}}$, the magnetic sensitivity can be further enhanced by improving the photon collection efficiency and by increasing the V_{Si}^- concentration. Simin *et al.* have suggested that the V_{Si}^- magnetic sensitivity can reach below 100 fT/$\sqrt{\text{Hz}}$ when the collection efficiency is improved and the V_{Si}^- concentration is 4×10^{16} cm^{-3}.[52] It has also been reported that the sensitivity can be improved by optimizing the annealing parameters[25] and isotropic purification of SiC.[52,53] Here, we discuss how much the V_{Si}^-(k) concentration can be increased without any significant decoherence of the V_{Si}^-(k) spins to further improve the magnetic sensitivity. In this study, we have clarified that the V_{Si}^-(k) concentration can be increased to 6.0×10^{16} cm^{-3} without any significant decoherence. On the other hand, Lekavicius *et al.* have reported that no significant decoherence of V_{Si}^- spins occurs at the fluence of 3×10^{18} cm^{-2} in the case of naturally abundant SiC, whereas the coherence time of V_{Si}^- spins in isotopically purified SiC after irradiation at 3×10^{18} cm^{-2}, which was several times higher than that in naturally abundant SiC, was reduced with increasing electron irradiation fluence due to the accumulation of paramagnetic defects.[53] This indicates that the effects of paramagnetic defects induced by electron irradiation are less significant compared to naturally abundant ^{13}C (1.07%, nuclear spin number I = 1/2) and ^{29}Si (4.67%, I = 1/2) isotopes. From the above facts, we roughly estimate that the V_{Si}^- (k) concentration that can be increased in naturally abundant SiC without significant coherence degradation (i.e., loss of magnetic sensitivity) is $\sim 2 \times 10^{17}$ cm^{-3} (2 MeV electron irradiation fluence of $\sim 5 \times 10^{19}$ cm^{-2}).

In the case of 2 MeV electron irradiation into SiC, the fluence of 1.3×10^{19} cm^{-2} (the highest fluence in this study) is converted to 5.4×10^{-4} dpa (displacement per atom) (see the supplementary material for detailed calculations). The mass density of 3.21 g/cm^3 and the displacement threshold energies of 25 eV for Si and 21 eV for C were used for the calculation,[54] although slightly different values have also been reported.[55–57] This value means that 0.054% of the lattice atoms are displaced once by electron bombardment. Considering that the critical dose for amorphization is 0.2 dpa,[58,59] this value is still low to cause defect clustering and amorphization. In other words, there is still room to increase the V_{Si}^-(k) concentration, and thus, the concentration above 2×10^{17} cm^{-3} is achievable while maintaining the crystallinity in the SiC lattice by electron irradiation.

IV. SUMMARY

We demonstrated the high-temperature operation of V_{Si}^--based magnetic sensors at least above 591 K by analyzing the effects of temperature on the ODMR spectra of V_{Si}^- defects in 4H-SiC created by high-energy electron irradiation. Although the V_{Si}^- concentration decreased by about 70% after annealing at 600 °C, the magnetic sensitivity was retained to a considerable extent. This suggests that the V_{Si}^- magnetic sensors can be used in high-temperature environments, such as interior planetary exploration, where the sensors are exposed to about 450 °C. In addition, we successfully characterized the V_{Si}^- concentration by room temperature ESR measurements and found that V_{Si}^- defects were created in proportion to the electron fluence up to the concentration of 6.0×10^{16} cm^{-3}. Stable photon emission from V_{Si}^-(k) defects by optical pumping and spin manipulation by RF application were possible at high temperatures, although the ODMR contrast decreased with increasing temperature. We also found that the change in the ODMR spectrum due to the Zeeman splitting was temperature-independent at least up to 591 K. This unique property is advantageous for magnetic sensors operating at thermal cycling conditions, such as space, since no measurement temperature calibration by resonance frequency adjustment is required. Our results pave the way for practical applications of V_{Si}^--based magnetic sensors operating under harsh environments, such as space and underground.

SUPPLEMENTARY MATERIAL

See the supplementary material for (1) characterization of V_{Si}^-(k) concentration, (2) distance and depth dependence of ODMR spectra, (3) sample variations on the temperature dependence of PL intensities, (4) ODMR spectra of the maximum fluence in this study, (5) radiation resistance of ODMR properties of V_{Si}^-, and (6) detailed calculation of the displacement per atom (dpa).

ACKNOWLEDGMENTS

This work was based on the results obtained from a NEDO Feasibility Study Program (Uncharted Territory Challenge 2050). Part of this study was supported by the MEXT Q-LEAP (Grant No. JPMXS0118067395) and the JSPS KAKENHI (Grant No. 20H00355) and was carried out within the framework of IAEA CRP F11020. We would like to thank Ms. Noriko Negishi for her technical support.

AUTHOR DECLARATIONS

Conflict of Interest

The authors have no conflicts to disclose.

Author Contributions

Shu Motoki: Data curation (equal); Formal analysis (equal); Investigation (equal); Writing – original draft (lead). **Shin-ichiro Sato:** Conceptualization (lead); Data curation (equal); Formal analysis (equal); Funding acquisition (lead); Investigation (equal); Supervision (lead). **Seiichi Saiki:** Formal analysis (equal); Investigation (equal); Methodology (equal); Writing – review & editing (lead). **Yuta Masuyama:** Methodology (equal); Writing – review & editing (equal). **Yuichi Yamazaki:** Writing – review & editing (equal). **Takeshi Ohshima:** Resources (equal); Supervision (lead); Writing – review & editing (lead). **Koichi Murata:** Formal analysis (equal); Funding acquisition (equal); Investigation (equal); Methodology (equal). **Hidekazu Tsuchida:** Resources (equal). **Yasuto Hijikata:** Supervision (lead); Writing – review & editing (lead).

DATA AVAILABILITY

The data that support the findings of this study are available from the corresponding author upon reasonable request.

REFERENCES

[1] H. Kraus, V. A. Soltamov, D. Riedel, S. Vath, F. Fuchs, A. Sperlich, P. G. Baranov, V. Dyakonov, and G. V. Astakhov, Nat. Phys. **10**, 157–162 (2014).
[2] H. Kraus, V. A. Soltamov, F. Fuchs, D. Simin, A. Sperlich, P. G. Baranov, G. V. Astakhov, and V. Dyakonov, Sci. Rep. **4**, 5303 (2014).
[3] F. Fuchs, B. Stender, M. Trupke, D. Simin, J. Pflaum, V. Dyakonov, and G. V. Astakhov, Nat. Commun. **6**, 7578 (2015).
[4] C. Kurtsiefer, S. Mayer, P. Zarda, and H. Weinfurter, Phys. Rev. Lett. **85**, 290–293 (2000).
[5] G.-Q. Liu, X. Feng, Q. Li, and R.-B. Liu, Nat. Commun. **10**, 1344 (2019).
[6] V. M. Acosta, E. Bauch, M. P. Ledbetter, A. Waxman, L.-S. Bouchard, and D. Budker, Phys. Rev. Lett. **104**, 070801 (2010).
[7] J. F. Barry, J. M. Schloss, E. Bauch, M. J. Turner, C. A. Hart, L. M. Pham, and R. L. Walsworth, Rev. Mod. Phys. **92**, 015004 (2020).
[8] D. M. Toyli, D. J. Christle, A. Alkauskas, B. B. Buckley, C. G. Van de Walle, and D. D. Awschalom, Phys. Rev. X **2**, 031001 (2012).
[9] P. G. Baranov, A. P. Bundakova, and A. A. Soltamova, Phys. Rev. B **83**, 125203 (2011).
[10] N. Mizuochi, S. Yamasaki, H. Takizawa, N. Morishita, T. Ohshima, H. Itoh, and J. Isoya, Phys. Rev. B **66**, 235202 (2002).
[11] N. Mizuochi, S. Yamasaki, N. Morishita, T. Ohshima, H. Itoh, T. Umeda, and J. Isoya, Phys. Rev. B **72**, 235208 (2005).
[12] M. Widmann, S.-Y. Lee, T. Rendler, N. T. Son, H. Fedder, S. Paik, L.-P. Yang, N. Zhao, S. Yang, I. Booker, A. Denisenko, M. Jamali, S. A. Momenzadeh, I. Gerhardt, T. Ohshima, A. Gali, E. Janzén, and J. Wrachtrup, Nat. Mater. **14**, 164–168 (2015).
[13] J. Senzaki, S. Hayashi, Y. Yonezawa, and H. Okumura, in *IEEE International Reliability Physics Symposium (IRPS), Burlingame, CA* (IEEE, Piscataway, NJ, 2018), pp. 3B.3-1–3B.3-6.
[14] M. Musolino, X. Xu, H. Wang, V. Rengarajan, I. Zwieback, G. Ruland, D. Crippa, M. Mauceri, M. Calabretta, and A. Messina, Mater. Sci. Semicond. Process. **135**, 106088 (2021).
[15] S. Asada, K. Murata, and H. Tsuchida, Appl. Phys. Express **15**, 045502 (2022).
[16] J. Li, G. Yang, X. Liu, H. Luo, L. Xu, Y. Zhang, C. Cui, X. Pi, D. Yang, and R. Wang, J. Phys. D: Appl. Phys. **55**, 463001 (2022).
[17] M. Radulaski, M. Widmann, M. Niethammer, J. L. Zhang, S.-Y. Lee, T. Rendler, K. G. Lagoudakis, N. T. Son, E. Janzen, T. Ohshima, J. Wrachtrup, and J. Vuckovic, Nano Lett. **17**, 1782–1786 (2017).
[18] D. M. Lukin, C. Dory, M. A. Guidry, K. Y. Yang, S. D. Mishra, R. Trivedi, M. Radulaski, S. Sun, D. Vercruysse, G. H. Ahn, and J. Vuckovic, Nat. Photonics **14**, 330–334 (2020).
[19] Y. Abe, A. Chaen, M. Sometani, S. Harada, Y. Yamazaki, T. Ohshima, and T. Umeda, Appl. Phys. Lett. **120**, 064001 (2022).
[20] C. J. Cochrane, J. Blacksberg, M. A. Anders, and P. M. Lenahan, Sci. Rep. **6**, 37077 (2016).
[21] Y. Yamazaki, Y. Chiba, T. Makino, S.-I. Sato, N. Yamada, T. Satoh, Y. Yijikata, K. Kojima, S.-Y. Lee, and T. Ohshima, J. Mater. Res. **33**, 3355–3361 (2018).
[22] T. M. Hoang, H. Ishiwata, Y. Masuyama, Y. Yamazaki, K. Kojima, S.-Y. Lee, T. Ohshima, T. Iwasaki, D. Hisamoto, and M. Hatano, Appl. Phys. Lett. **118**, 044001 (2021).
[23] M. Rühl, C. Ott, S. Gotzinger, M. Krieger, and H. B. Weber, Appl. Phys. Lett. **113**, 122102 (2018).
[24] J.-F. Wang, Q. Li, F.-F. Yan, H. Liu, G.-P. Guo, W.-P. Zhang, X. Zhou, L.-P. Guo, J.-M. Cui, X.- Ye Xu, J.-S. Xu, C.-F. Li, and G.-C. Guo, ACS Photonics **6**, 1736–1743 (2019).
[25] Y. Chiba, Y. Yamazaki, T. Makino, S.-I. Sato, N. Yamada, T. Satoh, K. Kojima, S.-Y. Lee, Y. Hijikata, and T. Ohshima, Mater. Sci. Forum **1004**, 337 (2020).
[26] M. H. Acuna, Rev. Sci. Instrum. **73**, 3717–3736 (2002).
[27] M. Hassanalian, D. Rice, and A. Abdelkefi, Prog. Aerosp. Sci. **97**, 61–105 (2018).
[28] H. Tsuchida, I. Kamata, T. Miyaza, M. Ito, X. Zhang, and M. Nagano, Mater. Sci. Semicond. Process. **78**, 2–12 (2018).
[29] T. C. Hain, F. Fuchs, V. A. Soltamov, P. G. Baranov, G. V. Astakhov, T. Hertel, and V. Dyakonov, J. Appl. Phys. **115**, 133508 (2014).
[30] E. Janzen, A. Gali, P. Carlsson, A. Gallsrom, B. Magnusson, and N. T. Son, Phys. B **404**, 4354–4358 (2009).
[31] V. Ivady, J. Davidsson, N. T. Son, T. Ohshima, I. A. Abrikosov, and A. Gali, Phys. Rev. B **96**, 161114 (2017).
[32] C. Kasper, D. Klenkert, Z. Shang, D. Simin, A. Gottscholl, A. Sperlich, H. Kraus, C. Schneider, S. Zhou, M. Trupke, W. Kada, T. Ohshima, V. Dyakonov, and G. V. Astakhov, Phys. Rev. Appl. **13**, 044054 (2020).
[33] M. E. Bathen, A. Galeckas, J. Müting, H. M. Ayedh, U. Grossner, J. Coutinho, Y. K. Frodason, and L. Vines, NPJ Quantum Inf. **5**, 111 (2019).
[34] R. Karsthof, M. E. Bathen, A. Galeckas, and L. Vines, Phys. Rev. B **102**, 184111 (2020).
[35] G. Alfieri and A. Mihaila, J. Phys.: Condens. Matter **32**, 465703 (2020).
[36] J. Coutinho, J. D. Gouveia, T. Makino, T. Ohshima, Ž Pastuović, L. Bakrač, T. Brodar, and I. Capan, Phys. Rev. B **103**, L180102 (2021).
[37] H. K. Nielsen, A. Hallén, D. M. Martin, and B. G. Svensson, Mater. Sci. Forum **483-485**, 497–500 (2005).
[38] H. K. Nielsen, A. Hallén, and B. G. Svensson, Phys. Rev. B **72**, 085208 (2005).
[39] P. Hazdra and J. Vobecký, Phys. Status Solidi A **216**, 1900312 (2019).
[40] T. Knezevic, A. Hadzipasic, T. Ohshima, T. Makino, and I. Capan, Appl. Phys. Lett. **120**, 252101 (2022).
[41] N. T. Son and I. G. Ivanov, J. Appl. Phys. **129**, 215702 (2021).

[42]K. D. Jahnke, A. Sipahigil, J. M. Binder, M. W. Doherty, M. Metsch, L. J. Rogers, N. B. Manson, M. D. Lukin, and F. Jelezko, New J. Phys. **17**(4), 043011 (2015).
[43]K. Danno, D. Nakamura, and T. Kimoto, Appl. Phys. Lett. **90**(20), 202109 (2007).
[44]P. B. Klein, R. Myers-Ward, K. K. Lew, B. L. VanMil, C. R. Eddy, D. K. Gaskill, A. Shrivastava, and T. S. Sudarshan, J. Appl. Phys. **108**(3), 033713 (2010).
[45]P. B. Klein, J. Appl. Phys. **103**(3), 033702 (2008).
[46]S.-I. Sato, T. Honda, T. Makino, Y. Hijikata, S.-Y. Lee, and T. Ohshima, ACS Photonics **5**(8), 3159–3165 (2018).
[47]V. A. Soltamov, A. A. Soltamova, P. G. Baranov, and I. I. Proskuryakov, Phys. Rev. Lett. **108**, 226402 (2012).
[48]J.-F. Wang, F.-F. Yan, Q. Li, Z.-H. Liu, J.-M. Cui, Z.-D. Liu, A. Gali, J.-S. Xu, C.-F. Li, and G.-C. Guo, Nat. Commun. **12**, 3223 (2021).
[49]F.-F. Yan, J.-F. Wang, Q. Li, Z.-D. Cheng, J.-M. Cui, W.-Z. Liu, J.-S. Xu, C.-F. Li, and G.-C. Guo, Phys. Rev. Appl. **10**, 044042 (2018).
[50]J. B. S. Abraham, C. Gutgsell, D. Todorovski, S. Sperling, J. E. Epstein, B. S. Tien-Street, T. M. Sweeney, J. J. Wathen, E. A. Pogue, P. G. Brereton, T. M. McQueen, W. Frey, B. D. Clader, and R. Osiander, Phys. Rev. Appl. **15**, 064022 (2021).
[51]W. Liu, Z.-P. Li, Y.-Z. Yang, S. Yu, Y. Meng, Z.-A. Wang, Z.-C. Li, N.-J. Guo, F.-F. Yan, Q. Li, J.-F. Wang, J.-S. Xu, Y.-T. Wang, J.-S. Tang, C.-F. Li, and G.-C. Guo, ACS Photonics **8**, 1889–1895 (2021).
[52]D. Simin, V. A. Soltamov, A. V. Poshakinsiy, A. N. Anisimov, R. A. Babunts, D. O. Tolmachev, E. N. Mokhov, M. Trupke, S. A. Tarasenko, A. Sperlish, P. G. Baranov, V. Dyakonov, and G. V. Astakhov, Phys. Rev. X **6**, 031014 (2016).
[53]I. Lekavicius, R. L. Myers-Ward, D. J. Pennachio, J. R. Hajzus, D. K. Gaskill, A. P. Purdy, A. L. Yeats, P. G. Brereton, E. R. Glaser, T. L. Reinecke, and S. G. Carter, PRX Quantum **3**, 010343 (2022).
[54]J. W. Steeds, G. A. Evans, L. R. Danks, S. Furkert, W. Voegeli, M. M. Ismail, and F. Carosella, Diamond Relat. Mater. **11**(12), 1923–1945 (2002).
[55]A. L. Barry, B. Lehmann, D. Fritsch, and D. Braunig, IEEE Trans. Nucl. Sci. **38**(6), 1111–1115 (1991).
[56]J. Lefèvre, J.-M. Costantini, S. Esnouf, and G. Petite, J. Appl. Phys. **105**(2), 023520 (2009).
[57]S.-I. Sato, T. Narahara, Y. Abe, Y. Hijikata, T. Umeda, and T. Ohshima, J. Appl. Phys. **126**, 083105 (2019).
[58]T. Seyller, R. Graupner, N. Sieber, K. V. Emtsev, L. Ley, A. Tadich, J. D. Riley, and R. C. G. Leckey, Phys. Rev. B **71**, 245333 (2005).
[59]L. B. Bayu Aji, T. T. Li, J. B. Wallace, and S. O. Kucheyev, J. Appl. Phys. **121**(23), 235106 (2017).